Iqbal, F.; Pyczak, F.; Neumeier, S.; Goeken, M.:
Crack nucleation and elastic / plastic deformation of TiAl alloys investigated by in-situ loaded atomic force microscopy
In: Materials Science and Engineering A (2017) Elsevier

DOI: 10.1016/j.msea.2017.02.017

Crack nucleation and elastic / plastic deformation of TiAl alloys investigated by in-situ loaded atomic force microscopy

F. Iqbal, F. Pyczak*, S. Neumeier and M Göken

Friedrich-Alexander-Universität Erlangen-Nürnberg (FAU), Materials Science and Engineering, Institute I, Germany

****Helmholtz-Zentrum Geesthacht, Institute of Materials Research, Germany***

Abstract

The crack propagation mechanisms of γ-titanium aluminides with fully lamellar microstructure have been studied using in-situ deformation in the Atomic Force Microscope (AFM). AFM demonstrated the unique capability to detect elastic as well as plastic deformation during in-situ tests from topography changes on the surface. It was found that the crack nucleation, which can occur at γ/γ and α_2/γ interfaces as well as inside the γ-phase, is always preceded by strong local elastic deformation. No cracking inside the α_2-phase was observed. The elastic and plastic deformation was confined inside the γ-phase and especially pronounced near interfaces which can be explained by the differences of the elastic and plastic deformation behavior of the γ- and α_2- phase.

Introduction

γ-TiAl alloys are attractive structural materials for applications in the temperature range up to 750 °C due to their high specific strength at these temperatures [1-5]. Nevertheless, they also suffer from brittleness and limited damage tolerance at ambient temperatures [6-11]. Thus, mechanisms of crack nucleation and propagation were frequently investigated in those alloys [12-21]. Both crack nucleation and propagation in most engineering TiAl-alloys are governed by the two phase microstructure.

This microstructure is composed of two intermetallic constituents, the ordered hexagonal α_2- and tetragonal γ-phase ($D0_{19}$ and $L1_0$ crystal structure, respectively). Frequently these two phases are arranged as parallel lamellae with distances of the lamellar interfaces in the range of some ten

nanometers up to several microns. Those lamellar microstructures exhibit a better creep strength compared to globular microstructure variants which also contain single phase γ-grains. The crystallographic plane of the lamellar interface is the {111} plane for the γ- and the (0001)-basal plane for the α_2-phase. In such lamellar structures frequently also γ/γ-lamellar interfaces are found sharing a twin or pseudo twin relationship with the neighboring γ-lamella with a common crystallographic {111} plane being the habit plane of the twin as well as the lamellar interface or an order-fault boundary [22].

As the $L1_0$ structure of the γ-phase constitutes a packing of alternating Ti- and Al-layers along the [001] direction (also termed c-direction) plastic deformation by ordinary dislocations of the type a/2<110]{111} does not destroy the ordering of the alternating Ti and Al layers. Plastic deformation with a displacement component along the ordered direction of alternating Ti- and Al-layers is either possible via a<101]{111} superdislocations (frequently splitting up in partial dislocations) or deformation twins with a/6<112> twinning partials and a {111} habit plane of the twin [22].

The crack propagation in γ -TiAl alloys was thoroughly investigated in the past including a large number of investigations utilizing in-situ experiments in the Scanning Electron Microscope (SEM) and Transmission Electron Microscope (TEM) (e.g. [12-21,23,24]). Nevertheless, some aspects as the interaction of the crack tip with γ/γ and α_2/γ lamellar interfaces and the elastic-plastic field in front of the crack tip are still not fully understood. To address these questions in-situ tensile and bending tests were carried out under Atomic Force Microscope (AFM) observation. AFM investigations have been also shown to be very successful in tracking dislocation emission processes at crack tips in NiAl [25]. The application of this microscopy technique for in-situ tests is novel in γ-TiAl alloys and can give new insights especially with respect to the elastic deformation in the crack tip vicinity as will be shown in this work.

Experimental details

The alloys under investigation were a cast and HIP Ti-45Al-1Cr alloy-and a Ti-48Al polysynthetically twinned (PST) crystal (all atomic percent). More information on the microstructure and heat treatments is given in the references [26,27]. Both alloys exhibit a lamellar microstructure.

In-situ loading of tensile and bending specimens was done using a Kammrath &Weiss tensile stage. The force resolution of the employed load cell was 1 N and the extension was measured by a build-in inductive displacement transducer. This stage was modified by a lab built special inset to perform also three or four point bending tests (see Fig. 1). All tests were performed at a displacement speed of 0.5 µm/s. In-situ observation of the loaded specimens was done using a Digital Instruments Dimension 3100 atomic force microscope (AFM).

Tensile specimens with dimensions of 20 mm × 5 mm × 1 mm were machined by wire erosion, notched with a razor blade, grounded using 2400 grit SiC papers for the last step, and finally chemical-mechanically polished with a mixture of 90 parts of colloidal silica (Struers OP-S) and 10 parts of hydrogen peroxide (30% Vol.). Four point bending specimens with dimensions of 15 mm x 2.5 mm x 1mm were machined via wire cutting using a diamond wire saw. Surface preparation and preparation of the notch for bending specimens was done similar to the method described above for tensile specimens. The gauge length in the case of tensile specimens was 15 mm while the specimens subjected to four point bending tests had 9 mm and 3 mm major and minor spans.

Results and discussion

Lamellar topographic contrast

Topographic lamellar contrast for both α_2- and γ-phase under AFM depends on the surface preparation method. In Fig. 2(a), topographic height contrast of an electro-polished lamellar microstructure is shown and in Fig. 2(b), the topographic height contrast of a lamellar microstructure prepared by chemical-mechanical polishing is illustrated. The topographic height contrast in the case of the electro-polished specimen shows higher removal rate for the α_2-phase than for the γ–phase. This is the reason why in figure 2(a) the α_2 lamellae show darker contrast. In this case the topographic height difference

between α_2- and γ-phase is around 50-70 nm which also depends on the electro-polishing parameters. In the case of the chemical-mechanical polishing the topographic height contrast is opposite as can be seen in Fig. 2(b). Now α_2 lamellae appear brighter and thus are topographically higher than the γ-lamellae. In this case the polished surfaces show very slight topographic contrast difference between α_2 and γ-phases which is of the order of 10-20 nm. In our tests we used chemical-mechanically polished surfaces in order to detect very slight elastic/plastic deformation occurring in the vicinity of the crack tip. A mirror type smooth surface is only achievable with the chemical-mechanical polishing technique which could also result in better scans as AFM is highly sensitive to surface roughness.

Plastic deformation

Prominent features of the microstructure under AFM observation are the traces of plastic deformation in the γ-phase. Fig. 3 shows AFM scans recorded at the same position in the crack tip vicinity at different applied loads and elongations. On the micrograph in Fig. 3(a) some traces of plastic deformation are absent which are visible as additional sharp steps in Fig. 3(b) recorded at higher load. This demonstrates that plastic deformation still takes place while the crack is propagating during the in-situ experiments and the crack propagation is not purely brittle. The character of this plastic deformation, either twinning or dislocation slip, cannot be deduced from the AFM micrographs as both mechanisms operate on {111} crystallographic planes and accordingly glide planes as well as twin habit planes appear under the same angle at the specimen surface.

Local plastic deformation and crack Initiation

The interlamellar semi-coherent α_2/γ interfaces, the closed packed {111} planes of the γ-phase and the γ/γ interfaces are known from literature as preferential paths for crack propagation [28]. But they also act as crack nucleation sites. One well known reason for this is the energy of internal interfaces in TiAl favoring decohesion on γ/γ and to a lesser extent on α_2/γ interfaces [29]. Additionally it was found in TEM-investigations that plastic deformation by dislocation slip and twinning is hindered by internal γ/γ and α_2/γ interfaces [30]. This is supposed to generate internal stresses at the interfaces leading to microcrack nucleation. In this work it is observed that the crack initiation in all three cases (closed

packed plane, γ/γ and α_2/γ interface) was preceded by local depressions in the topography at the subsequent crack opening site. These depressions are often deeper than topographic features connected with traces of plastic deformation which are also normally present in the vicinity of the crack tip or lamellar interfaces. In addition topographic features connected with traces of plastic deformation or lamellar interfaces appear as distinct steps or ridges while these depressions are more gradual and are supposed to represent local elastic strain concentrations. Examples for such local elastic depressions will be shown and discussed in detail later. The nucleation of new cracks is also often connected with the interaction of deformation bands with α_2/γ lamellar interfaces when strong plastic deformation is found in the γ-TiAl lamellae. In Fig. 4(a) distinct surface steps from deformation bands are detected by the AFM inside the γ-lamellae while such steps are absent in the neighboring α_2-Ti_3Al lamella. This is also visible in the section analysis parallel to the α_2-lamella which is marked (1) in Fig. 4(a). Due to the fact that plastic deformation at least in directions leading to significant topographic features on the surface like the steps observed in the neighboring γ-lamellaeare absent in the α_2-phase, large height differences can occur between plastically deformed γ-phase and undeformed α_2-phase. By comparing two section analyses across the γ/α_2 interface, one above the position where a deformation band occurs in the γ-phase which is marked (2) and the other below this position marked as (3), it is clear that while both phases are nearly at the same height above the deformation band a large height drop has developed at the γ/α_2 interface between the deformed region of the γ-lamellae and the α_2-lamellae. It is open to speculation in which way these incompatibilities in deformation are negotiated. Possibilities are elastic deformation of the α_2 phase, local plastic deformation at the γ/α_2 interface or already decohesion of the γ/α_2 interface. Small cracks at the interface caused by the latter may be not detected by AFM due to the finite tip radius and can act as initiation sites for larger cracks at the α_2/γ lamellar interfaces.

With respect to surface energy γ/γ interfaces should be preferred sites for crack nucleation and propagation [3]. Nevertheless, cracks are observed to also nucleate inside the γ-phase or at interlamellar boundaries, but not inside the α_2-phase and crack initiation and propagation at γ/α_2-interfaces are often found. This can be explained with the help of the elastic/plastic incompatibility of

both phases. According to literature the Young's modulus of the γ-phase is higher than that of the α_2-phase [28] but the yield strength of the α_2-phase is higher than that of the γ-phase. Due to this the onset of plastic deformation in the softer γ-phase is easier. This plastic incompatibility plays a role at the coherent γ/α_2-interfaces where the different deformation behavior of both phases produces high surface steps as possible crack openings as shown in Fig. 4. In addition to its lower yield point another effect could also support an earlier plastic deformation of the γ-phase compared to the α_2-phase. It is known from literature that the interatomic distances at the coherent or in most cases semi-coherent (i.e. presence of interfacial dislocations) γ/α_2-lamellar interface are slightly different and induce compressive coherency stresses in the α_2-phase while tensile stresses are found in the γ-phase [31]. With their tensile character in the γ-phase the coherency stresses can add up with externally applied tensile stresses and hence the γ-phase locally reaches its yield point while the externally applied load is still below the yield point of the whole γ/α_2-compound. On the contrary the α_2-phase contains compressive residual stresses which compensate the externally applied tensile stress partially or fully. Thus the α_2-phase remains under a lower stress level and accordingly shows no traces of plastic deformation on the surface. This should also lead to significant local stresses at the lamellar α_2/γ interface.

The confinement of plastic deformation to the γ-phase is also confirmed by EBSD mappings of the crack tip vicinity and similar areas in an undeformed specimen. The local misorientation is a measure for local plastic deformation in EBSD mappings. Fig. 5 shows a comparison of local misorientation contrast of an undeformed and a deformed specimen. In the deformed specimen in Fig. 5(a) the confinement of the plastic deformation at γ/α_2 interfaces, γ/γ twin interfaces as well as inside the γ-phase is visible but more or less no misorientation contrast is observable inside the α_2 –lamellae. In comparison the undeformed specimen in Fig. 5(b) shows more or less no local misorientation contrast in both phases. Hence these EBSD-measurements support the finding of the AFM-observations that plastic deformation is nearly exclusively confined to the γ-phase. As mentioned above the two possible reasons for this are the lower yield point of the γ-phase facilitating earlier plastic deformation and the

tensile coherency stresses present especially near the γ/α_2 interfaces leading to a higher local tensile stress level in the γ-phase if tensile external stress is applied.

These incompatibilities in plastic deformation between the γ- and the α_2-phase explain both the occurrence of significant displacements between deformed γ- and undeformed α_2-phase as well as the occurrence of stress concentrations at γ/α_2 interfaces. It is assumed that both phenomena play a role for crack initiation at these positions. Especially, the local stress concentrations can only be investigated by AFM in-situ tests because the contrast mechanism employed is only detectable in AFM. The possibility to vary the externally applied stress makes them distinguishable from other topographic features because their intensity varies with the external stress level as will be shown in the following section.

Elastic deformation in front of the crack tip

The interaction of the advancing crack tip with the internal interfaces was observed in-situ under the AFM in a PST-crystal. First the crack was extended under observation by an optical microscope in AFM until a desired position of the crack tip with respect to an internal interface was reached. At this point the specimen was partially unloaded and reloaded again under AFM observation to investigate the deformation field ahead of the crack tip. AFM investigations on crack tips in NiAl have been shown to clearly reveal elastic deformation and depression zones around cracks [32]. During loading an AFM scan was recorded at 230 N applied load. It shows localized distinct depression fields inside the γ lamella visible in the AFM scan in Fig. 6(a). In order to understand if this depression is caused by either elastic or plastic deformation the specimen was unloaded to 154 N. At this load again an AFM scan was taken which is shown in Fig. 6(b). It is clearly visible that due to unloading a big portion of the depression vanished. Therefore from these observations one can conclude that the strain which occurs at the arrested crack tip is of elastic nature because it is partly recovered during unloading. Nevertheless the overall appearance of the elastic strain field is similar in Fig. 6(a,b) with two elongated areas of localized elastic strain in a V-shape in front of the crack tip marked as A and B in Fig. 6(b). A strong elastic strain concentration is found at the adjacent γ/γ lamellar boundary at the positions where the strain fields ‘A’ and ‘B’ hit the lamellar interface. Between these elastic strain

fields a less deformed region is also present which is marked as ‘C’ in Fig. 6(b) and the strain at the lamellar interface is also reduced directly in front of the crack tip.

To investigate the elastic strain field in front of the crack tip in more detail, the specimen was again loaded from 154 N with small increments, until further crack advancement into the γ lamella takes place. The respective AFM micrographs are presented in Fig. 7 (a, b, c & d). It is clearly visible that the strain concentration becomes more pronounced with increasing load from 154 N over 186 N to 199 N. At a load of 229 N the crack propagates further into the γ-lamella and the elastic strain field is relaxed. Interestingly the intensity of strain in the upper and lower part of the V-shaped depression area is not equal but more pronounced in the part marked by ‘B’ in Fig. 6(b). The possible reasons for this asymmetry of the V-shaped depression area are either the crack not being oriented perfectly perpendicular but inclined with respect to the lamellar orientation and applied load or the anisotropy of plastic deformation in the γ lamella. This plastic deformation is evidenced by the parallel traces of deformation bands visible in all micrographs of Fig. 6 and 7. These are pronounced on one glide or twin plane but absent in the other. It is assumed that the yield strength is accordingly different in these two crystallographic directions. Such orientation dependent differences in yield stress due to the crystallographic anisotropy of the tetragonal $L1_0$ structure were reported by many authors [33,34,35]. They should result in more pronounced elastic strain fields in the one and less pronounced in the other direction when the material starts to deform plastically.

In order to characterize the elastic deformation in more detail and to clarify if the yield strength differs for the two elastic strain bands A and B the z-displacement in these two elastic strain bands was analyzed for different applied external loads. The process of analysis is illustrated in Fig. 8. Two respective locations and the corresponding line profile where a section analysis of the AFM micrographs was performed, marked with D (just ahead of the crack tip) and E (approximately 1 μm away from the crack tip), are shown. The depths of the elastic deformation bands A and B were measured as height differences between the lowest point of the deformation band and the highest point in the direct vicinity marked with arrow heads on the section analysis lines. The results plotted versus the applied external load are shown in Fig. 9(a) and (b). As already observed qualitatively in the AFM

micrographs the elastic deformation is less pronounced for band ‘A’. Directly in front of the crack tip (Fig. 9(a)) the intensity of elastic deformation is more or less unchanged irrespective of the externally applied load until the crack propagates further into the γ lamella which occurs at 229 N applied load leading to the relaxation of the elastic strain More distant from the crack tip the elastic deformation increases with increasing externally applied load until again the elastic strain is relaxed after further crack propagation as shown in Fig. 9(b). The elastic depression found here is probably the lateral contraction caused by the tensile stress field of the crack tip in the surface plane of the specimen. Directly in front of the crack tip the yield point is already reached and plastic deformation occurs. Thus the level of elastic deformation remains constant representing the yield point level. At a larger distance, where the stress level is lower the material can still deform elastically. It is interesting to note in this respect that the elastic distortion shown in Fig. 9(b) never exceeds the yield point level from Fig. 9(a). The analysis supports the assumption that the yield point is different for activation of plastic deformation in the bands ‘A’ and ‘B’. Thus, near the crack tip where the yield point is reached the asymmetry in the intensity of the elastic strain field is probably caused by different yield points for the different crystallographic directions in the γ-lamella. The combination of AFM with in-situ deformation as employed here is able to observe this effect directly. Further away from the crack tip where the yield point is neither exceeded in band ‘A’ nor in ‘B’ the asymmetry is most probably due to the crack not being perpendicular to the lamellar orientation.

Conclusions

1. Atomic force microscopy has been used successfully for in-situ crack propagation experiments to investigate the small elastic/plastic strain activity occurring due to local stress concentrations in the crack tip vicinity of TiAl alloys.

2. In addition to traces of plastic deformation crack initiation is preceded by local depressions in the surface at the subsequent crack opening site which represent local elastic strain concentrations.

3. The plastic deformation is confined inside the γ-phase which is thought to be an effect of the higher yield point of the α_2-phase and the tensile coherency stresses inside the γ-phase.

4. The propagation of cracks is preceded by elastic/plastic deformation in front of the crack tip. That the local yield stress for different crystallographic orientations of the tetragonal γ-phase differs and can lead to unsymmetrical elastic deformation fields in front of the crack tip was directly observed.

Acknowledgements

The authors acknowledge the financial support of German Science Foundation (DFG), Bonn under contract No: GO741/14-1.

References

[1] F. Appel, J.D.H. Paul, M. Oehring, Gamma Titanium Aluminde Alloys, 2011, Wiley-VCH, Weinheim.

[2] Y.-W. Kim, Journal of Metals 41 (1989) 24-30.

[3] M. Yamaguchi, H. Inui, Structural intermetallics 1993, TMS, Pittsburg, PA, p 127.

[4] Y.-W. Kim, D.M. Dimiduk, Journal of Metals 43 (1991) 40-47.

[5] M. Yamaguchi, Material Science Technology 8 (1992) 299-307.

[6] J. Zhang, J.D. Shi, D.X. Zou, Z.Y. Zhong, Scripta Mater 34 (1996)1815-1818.

[7] L.L. Rishel, N.E. Biery, R. Raban, V.Z. Gandelsman, T.M. Pollock, A.W. Cramb, Intermetallics 6 (1998) 629-36.

[8] N. Biery, M. De Graef in: Y.-W. Kim, D.M. Dimiduk, M.H. Loretto (editors): Gamma titanium aluminides. Warrendale, PA: Minerals Metals and Materials Society, 1999, p. 557-564.

[9] T.M. Pollock, D.R. Mumm, K. Muraleedharan, P.L. Martin, Scripta Mater. 35 (1996) 1311-1316.

[10] A. Gilchirst, T.M. Pollock in: K.J. Hemker, D.M. Dimiduk et al (editors): Warrendale, PA: TMS; 2001 P.3-12.

[11] R.I. Prihar in: K.J. Hemker, D.M. Dimiduk et al (editors): Structural intermetallics. Warrendale, PA: TMS, 2001, p.819-824.

[12] D. Häussler, U. Messerschmidt, M. Bartsch, F. Appel, R. Wagner, Materials Science and Engineering A 233 (1997) 15-25.

[13] Y. Wu, L. Zhen, D.Z. Yang, M.S. Kim, S.K. Hwang, Y. Umakoshi, Intermetallics 12 (2004) 43-45.

[14] Y.H. Lu, Y.G. Zhang, L.J. Qiao, Y.B. Wang, C.Q. Chen, W.Y. Chu, Intermetallics 8 (2000)1443-1445.

[15] Y.H. Lu, Y.G. Zhang, L.J. Qiao, Y.B. Wang, C.Q. Chen, W.Y. Chu, Materials Science and Engineering A 289 (2000) 91-98.

[16] K.F. Yao, J. Xiao, J. Zhang, Intermetallics 8 (2000) 569-573.

[17] P. Wang, N. Bathe, K.S: Chan, K.S. Kumar, Acta Materialia 51 (2003) 1573-1591.

[18] L.M. Hsiung, A.J. Schwarz, T.G. Nieh, Intermetallics 12 (2004) 727-732.

[19] R. Cao, H.J. Yao, J.H. Chen, J. Zhang, Materials Science and Engineering A 420 (2006) 122-134.

[20] S.W. Kim, K.S. Kumar, M.H. Oh, D.M. Wee, Intermetallics 15 (2007) 976-984.

[21] Y. Mine, K. Takashima, P. Bowen, Materials Science and Engineering A 532 (2012) 13– 20.

[22] F. Appel, R. Wagner, Materials Science and Engineering R 22 (1998) 187-268.

[23] R. Munoz-Moreno, C.J. Boehlert, M.T. Perez-Prado, E.M. Ruiz-Navas, J. Llorca, Metallurgical and Materials Transactions A 43 (2012) 1198-1208.

[24] R. Munoz-Moreno, M.T. Perez-Prado, J. Llorca, E.M. Ruiz-Navas, C.J. Boehlert, Metallurgical and Materials Transactions A 44 (2013) 1887-1896.

[25] F. Thome, M. Göken, H. Vehoff, Intermetallics 7 (1999) 491-499.

[26] S. Gebhard, F. Pyczak, M. Göken, Materials Science and Engineering A 523 (2009) 235-241.

[27] M. Riemer, H.G. Jentsch, H. Biermann, H. Mughrabi, Intermetallics 7 (1999) 241-249.

[28] S.J. Balsone, B.D: Worth, J.M. Larsen, J.W. Jones, Scripta Metallurgica et Materialia 32 (1995) 1653-1658.

[29] M. Kempf, M. Göken, H. Vehoff, Materials Science and Engineering A 320-331 (2002) 184-189.

[30] F.A. Guo, V. Ji, M. Francois, Y.G. Zhang, Acta Materialia 51 (2003) 5349-5358.

[31] P.M. Hazzledine, Intermetallics 6 (1998) 673-677.

[32] M. Göken, H. Vehoff, P. Neuman, J. Vac. Sci. & Technol. B 14 (1996) 1157-1161.

[33] H. Mecking, Ch. Hartig, U.F. Kocks, Acta Materialia 44 (1996) 1309-1321.

[34] D.M. Dimiduk, T.A. Parthasarathy, P.M. Hazzledine, Intermetallics 9 (2001) 875-882.

[35] R.A. Brockman, Int. J. Plasticity 19 (2003) 1749-1772.

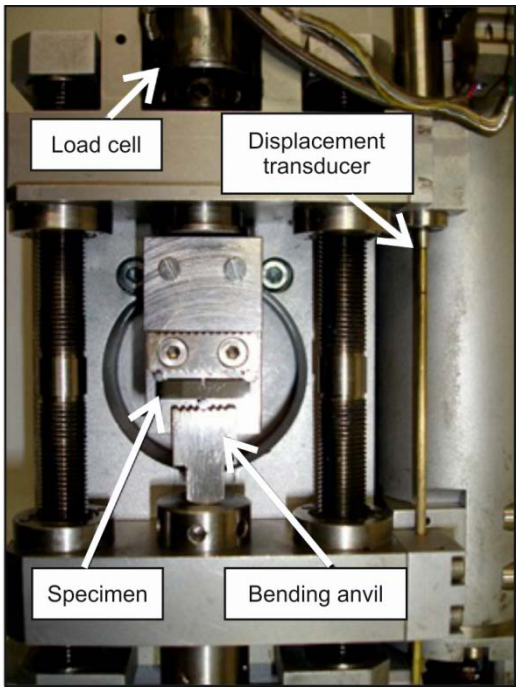

Fig. 1: Kammrath & Weiss tensile machine with laboratory built inset for in-situ 3- or 4-point bending tests under atomic force microscope observation

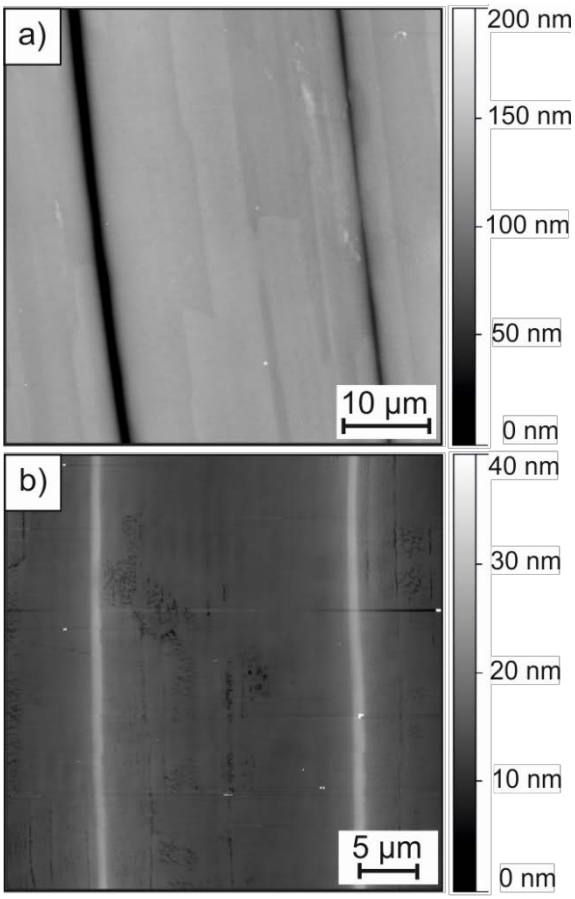

Fig. 2: AFM topographic contrast of TiAl-PST crystals (a) Electro polished (b) Chemical-mechanically polished

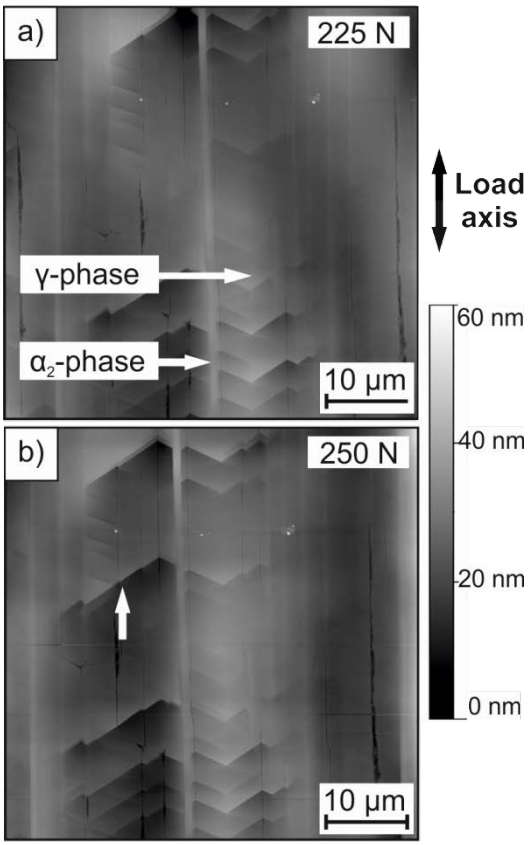

Fig. 3: Lamellar region in a TiAl-PST specimen at externally applied loads of 225 N (a) and 250 N (b); an additional shear band is marked by an arrow in (b).

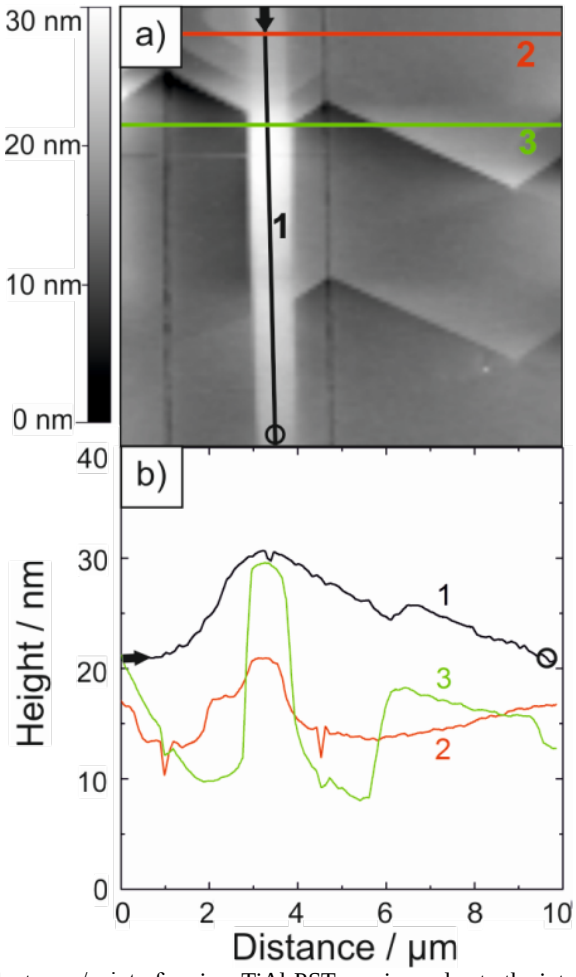

Fig. 4: Nucleation of a new crack at a α_2 / γ interface in a TiAl-PST specimen due to the interaction of a deformation band in the γ-phase (a), Line sections to (a) for lines marked with 1, 2 and 3 (orientation of line 1 indicated by circle and arrow) (b).

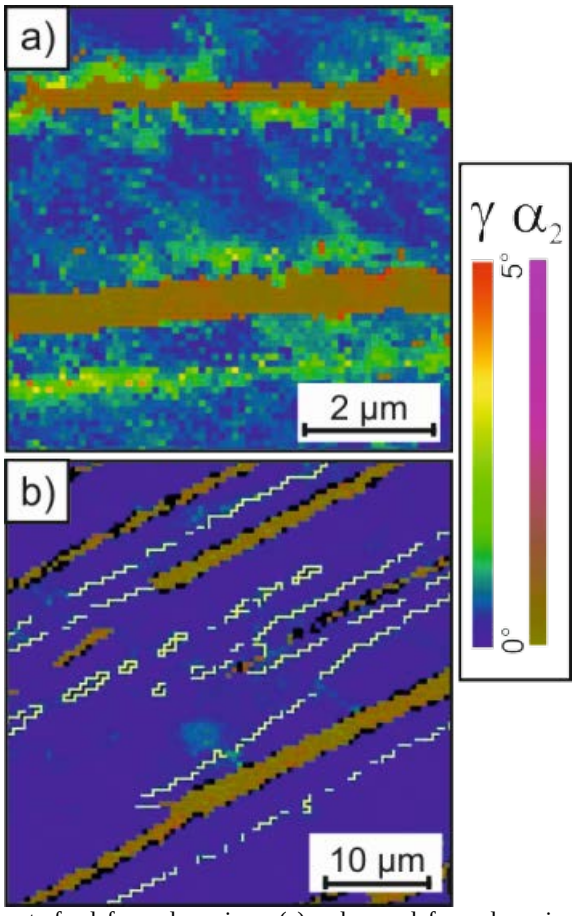

Fig 5: Local misorientation contrast of a deformed specimen (a) and an undeformed specimen (b) of Ti-45Al-1Cr recorded by EBSD. The legend shows the local misorientation in the phases γ and α_2, respectively.

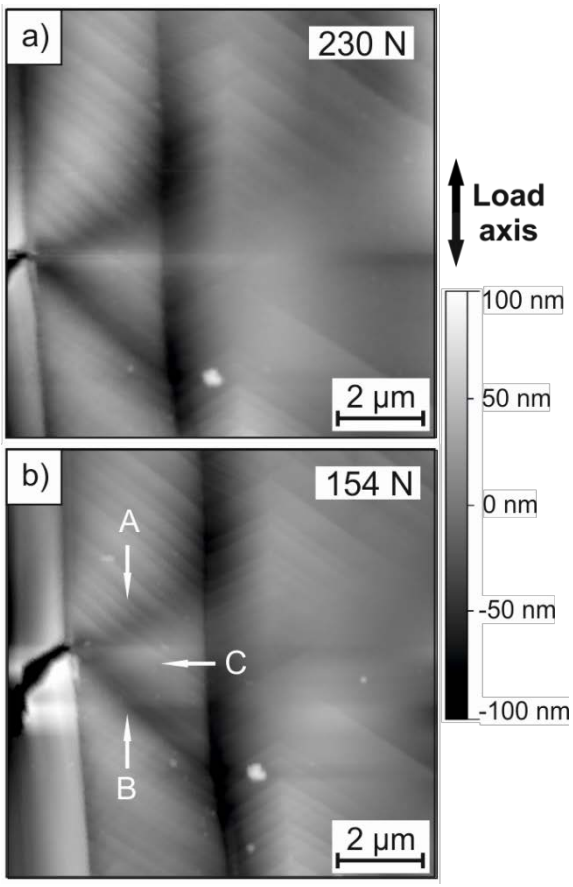

Fig. 6: AFM micrograph of a crack tip region in a TiAl-PST specimen under external load of 230 N (a) same location after unloading to 154 N (b).

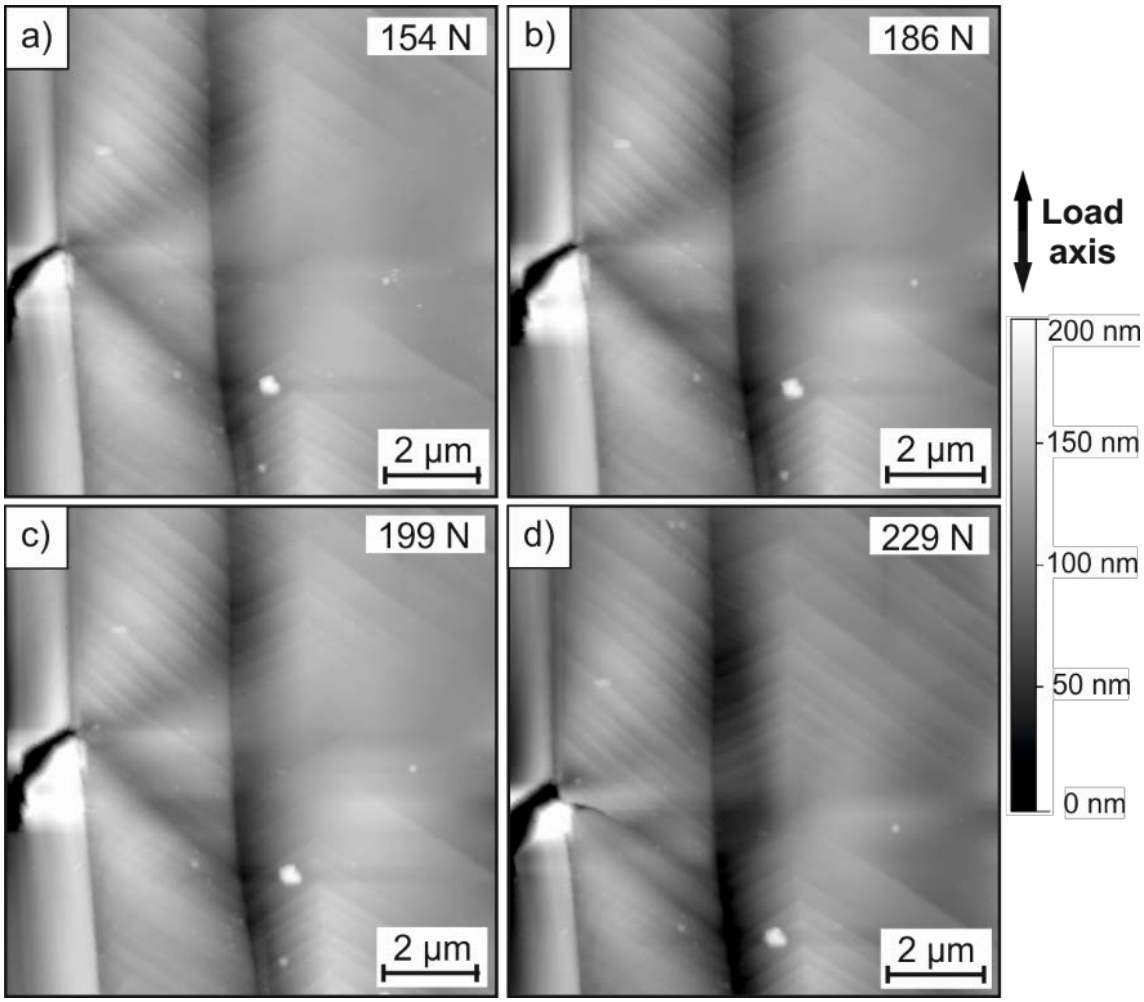

Fig. 7: AFM micrographs of a loaded crack tip in a TiAl-PST specimen under externally applied load of 154 N (a), 186 N (b), 199 N (c) and 229 N (d).

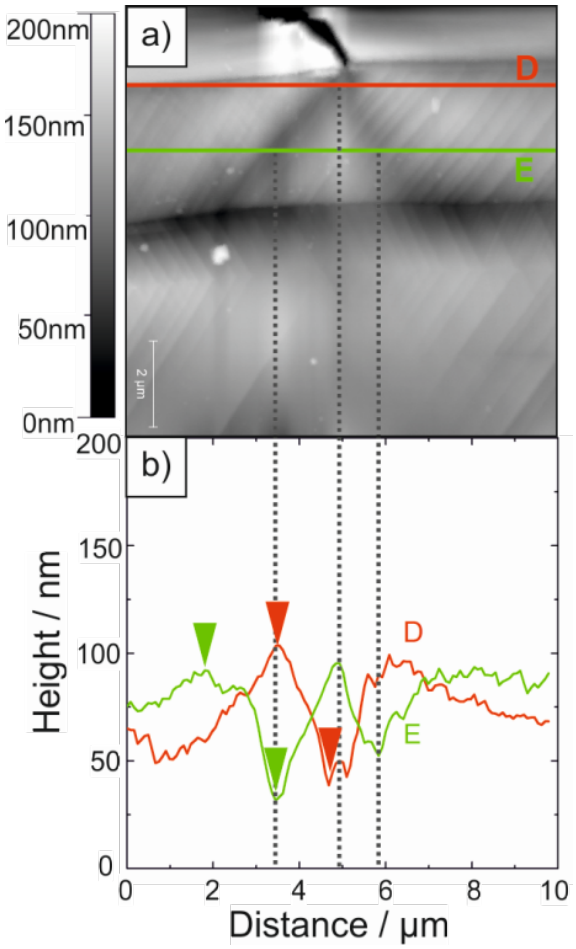

Fig. 8: Location of the section analysis ‘D’ just ahead of the crack tip and ‘E’ 1µm away from the crack tip (a), Section analysis lines show how the elastic deformation is calculated by taking the difference between the minima and the maxima of the respective line (b).

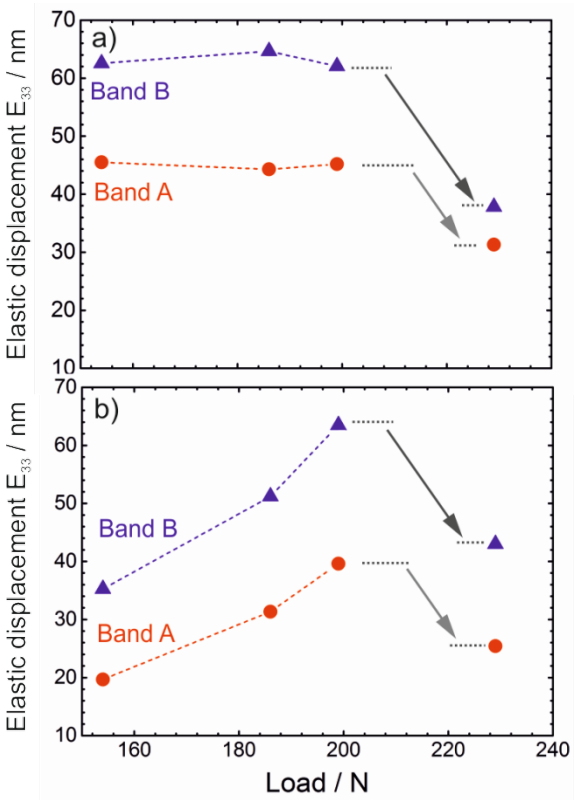

Fig. 9: Elastic displacement of the bands A and B marked in figure 6(b): (a) close to the crack tip (along line D as marked in Fig. 8); (b) at a larger distance from the crack tip (along line E as marked in Fig. 8).